Mon. Not. R. Astron. Soc. **377,** 1393–1406 (2007) doi:10.1111/j.1365-2966.2007.11687.x

The properties of Jovian Trojan asteroids listed in SDSS Moving Object Catalogue 3

Gy. M. Szabó,[1⋆†] Ž. Ivezić,[2] M. Jurić[3] and R. Lupton[3]

[1]*Department of Experimental Physics & Astronomical Observatory, University of Szeged, 6720 Szeged, Hungary*
[2]*Department of Astronomy, University of Washington, Seattle, WA 98155, USA*
[3]*Princeton University Observatory, Princeton, NJ 08544, USA*

Accepted 2007 February 28. Received 2007 February 27; in original form 2007 January 18

ABSTRACT

We analyse 1187 observations of about 860 unique candidate Jovian Trojan asteroids listed in the 3rd release of the Sloan Digital Sky Survey (SDSS) Moving Object Catalogue. The sample is complete at the faint end to $r = 21.2$ mag (apparent brightness) and $H = 13.8$ (absolute brightness, approximately corresponding to 10 km diameter). A subset of 297 detections of previously known Trojans were used to design and optimize a selection method based on observed angular velocity that resulted in the remaining objects. Using a sample of objects with known orbits, we estimate that the candidate sample contamination is about 3 per cent. The well-controlled selection effects, the sample size, depth and accurate five-band UV–IR photometry enabled several new findings and the placement of older results on a firmer statistical footing. We find that there are significantly more asteroids in the leading swarm (L4) than in the trailing swarm (L5): $N(\mathrm{L4})/N(\mathrm{L5}) = 1.6 \pm 0.1$, independently of limiting object's size. The overall counts normalization suggests that there are about as many Jovians Trojans as there are main-belt asteroids down to the same size limit, in agreement with earlier estimates. We find that Trojan asteroids have a remarkably narrow colour distribution (root mean scatter of only $\sim$0.05 mag) that is significantly different from the colour distribution of the main-belt asteroids. The colour of Trojan asteroids is correlated with their orbital inclination, in a similar way for both swarms, but appears uncorrelated with the object's size. We extrapolate the results presented here and estimate that the Large Synoptic Survey Telescope will determine orbits, accurate colours and measure light curves in six photometric bandpasses for about 100 000 Jovian Trojan asteroids.

Key words: astronomical data bases: miscellaneous – catalogues – minor planets, asteroids – Solar system: general.

1 INTRODUCTION

Jovian Trojan asteroids are found in two swarms around the L4 and L5 Lagrangian points of Jupiter's orbit (for a review see Marzari et al. 2001). The first Jovian Trojan was discovered a century ago by Max Wolf. Nearly 2000 Jovian Trojans were discovered by the end of 2003 (Bendjoya et al. 2004, hereafter B04). About half are numbered asteroids with reliable orbits (Marzari et al. 2001). Their total number is suspected to be similar to the number of the main-belt asteroids[1] (Shoemaker, Shoemaker & Wolfe 1989).

The Trojans' positions relative to Jupiter librate around L4 (leading swarm) and L5 (trailing swarm) with periods of the order of a hundred years. Their orbital eccentricity is typically smaller ($<$0.2) than those of main-belt asteroids, but the inclinations are comparable, with a few known Trojans (KTs) having inclinations larger than 30°. The largest objects have diameters exceeding 100 km. They typically have featureless (D-type) spectra and extremely low optical albedo (Tedesco 1989; Fernández, Sheppard & Jewitt 2003). These spectral properties are similar to those of cometary nuclei. However, there are also Trojans that have P or common C-type classification, mostly found in the trailing swarm (Fitzsimmons et al. 1994). The collisional grinding of Trojan asteroids is supported by their observed size distribution (Jewitt, Trujillo & Luu 2000, hereafter JTL).

Numerous studies of the origin of Jovian Trojans are based on two different hypothesis. According to one of them, the Jovian Trojans were formed simultaneously with Jupiter in the early phase of the solar nebula. The growing Jupiter could have captured and

⋆E-mail: szgy@titan.physx.u-szeged.hu
†Magyary Zoltán Postdoctoral Research Fellow.

[1] Recent work supports this claim. Ivezić et al. (2001) estimated that the number of main-belt asteroids with diameters larger than 1 km is 740 000, with a somewhat higher estimate by Tedesco, Cellino & Zappalá (2005), and Jewitt, Trujillo & Luu (2000) estimated that there are between 520 000 and 790 000 Jovian Trojans above the same size limit.

stabilized the plantesimals near its L4 and L5 points (Peale 1993). The other hypothesis assumes that the majority of Jovian Trojans were captured over a much longer period, and were formed either close to Jupiter, or were gravitationally scattered from the main belt or elsewhere in the Solar System (Jewitt 1996). The spectral comet-like appearance of many Trojans is consistent with the scattering from the outer Solar System.

Depending on the importance of gas drag when Trojans formed, the L4 and L5 swarms could have different dynamics. The presence of significant gas drag helps stabilize orbits around the L5 point. On the other hand, these trailing objects have later evolution different from the leading swarm because planetary migration destabilizes L5 (Gomes 1998). Morbidelli et al. (2005) recently suggested a more complex picture: the present permanent Trojan populations are built up by objects that were trapped after the 1:2 mean motion resonance crossing of the Saturn and the Jupiter. Therefore, it is possible that size distributions, or detailed distributions of orbital parameters, could be different for the leading and trailing swarm. However, no such differences have yet been found (Marzari et al. 2001, and references therein).

It is noteworthy that there are severe observational biases in the sample of known Jovian Trojans due to their large distance. For example, although the numbers of main-belt asteroids and Trojans to a given size limit are similar, only about 1 per cent of the known objects belong to the latter group. This is a consequence of the fact that a Trojan at a heliocentric distance of 5.2 au is about 4 mag fainter than a same-size main-belt asteroid at a heliocentric distance of 2.5 au (as observed in opposition, and not accounting for differences in albedo, which further diminishes the Trojan's apparent magnitude).

Here we present an analysis of the properties of about 1000 known and candidate Jovian Trojan asteroids based on the data collected by Sloan Digital Sky Survey (SDSS, York et al. 2000). SDSS, although primarily designed for observations of extragalactic objects, is significantly contributing to studies of the Solar System objects because asteroids in the imaging survey must be explicitly detected and measured to avoid contamination of the samples of extragalactic objects selected for spectroscopy. Preliminary analysis of SDSS commissioning data (Ivezić et al. 2001, hereafter I01) showed that SDSS will increase the number of asteroids with accurate five-colour photometry by more than two orders of magnitude, and to a limit about 5 mag fainter (7 mag when the completeness limits are compared) than previous multicolour surveys (e.g. The Eight Colour Asteroid Survey, Zellner, Tholen & Tedesco 1985). As we demonstrate below, the SDSS data extend the faint completeness limit for Trojan asteroids by about 1.5 mag (to a limiting diameter of $\sim$10 km).

The large sample and accurate astrometric and five-band photometric SDSS data to a much fainter limit than reached by most previous surveys, together with suitable ways to quantify selection effects, allow us to address the following questions.

(i) What is the size distribution of Jovian Trojans asteroids with diameters larger than 10 km?

(ii) Do the leading and trailing swarms have the same size distribution (including both the distribution shape and the overall number above some size limit)?

(iii) What is their colour distribution in the SDSS photometric system, and how does it compare to the colour distribution of main-belt asteroids?

(iv) Is the colour distribution correlated with inclination, as suggested by a preliminary analysis of SDSS data (Ivezić et al. 2002a, hereafter I02a)?

(v) Are the Trojans' size and colour correlated (as suggested by B04)?

(vi) Do the leading and trailing swarms have the same colour distribution?

(vii) Is the size distribution correlated with inclination?

The SDSS asteroid data are described in Section 2, and in Section 3 we describe a novel method for selecting candidate Jovian Trojan asteroids from SDSS data base. Analysis of the properties of selected objects, guided by the above questions, is presented in Section 4. We summarize our results in Section 5, and discuss their implications for the origin and evolution of Trojan asteroids.

2 SDSS OBSERVATIONS OF MOVING OBJECTS

SDSS is a digital photometric and spectroscopic survey using a dedicated 2.5 m telescope at the Apache Point Observatory, which will cover 10 000 deg^2 of the Celestial Sphere in the North Galactic cap, and a smaller ($\sim$225 deg^2) and deeper survey in the Southern Galactic hemisphere (Abazajian et al. 2003, and references therein). The survey sky coverage will result in photometric measurements for over 10^8 stars and a similar number of galaxies. The flux densities of detected objects are measured almost simultaneously (within $\sim$5 min) in five bands (u, g, r, i and z) with effective wavelengths of 3551, 4686, 6166, 7480 and 8932 Å (Fukugita et al. 1996; Gunn et al. 1998; Hogg et al. 2002; Smith et al. 2002). The photometric catalogues are 95 per cent complete for point sources to limiting magnitudes of 22.0, 22.2, 22.2, 21.3 and 20.5 in the North Galactic cap. Astrometric positions are accurate to about 0.1 arcsec per coordinate (rms) for sources brighter than 20.5$^{\rm m}$ (Pier et al. 2003), and the morphological information from the images allows robust star–galaxy separation (Lupton et al. 2001, 2002) to $\sim$21.5$^{\rm m}$. The photometric measurements are accurate to 0.02 mag (both absolute calibration, and rms scatter for sources not limited by photon statistics; Ivezić et al. 2004). The recent fifth public Data Release (DR5) includes imaging data for $\sim$8000 deg^2 of sky, and catalogues for 2.15×10^8 objects. For more details please see Abazajian et al. (2003) and references therein.

SDSS Moving Object Catalogue[2] (hereafter SDSS MOC) is a public, value-added catalogue of SDSS asteroid observations (Ivezić et al. 2002b, hereafter I02b). It includes all unresolved objects brighter than $r = 21.5$ and with observed angular velocity in the 0.05–0.5 deg d^{-1} interval. In addition to providing SDSS astrometric and photometric measurements, all observations are matched to known objects listed in the ASTORB file (Bowell 2001), and to a data base of proper orbital elements (Milani 1999), as described in detail by Jurić et al. (2002, hereafter J02). J02 determined that the catalogue completeness (number of moving objects detected by the software that are included in the catalogue, divided by the total number of moving objects recorded in the images) is about 95 per cent, and its contamination rate is about 6 per cent (the number of entries that are not moving objects, but rather instrumental artefacts).

The third release of SDSS MOC used in this work contains measurements for over 204 000 asteroids. The quality of these data was discussed in detail by I01, including a determination of the size and colour distributions for main-belt asteroids. An analysis of correlation between colours and asteroid dynamical families was presented by I02a. An interpretation of this correlation as the dependence of colour on family age (due to space weathering effect) was proposed

[2] Available at http://www.sdss.org.

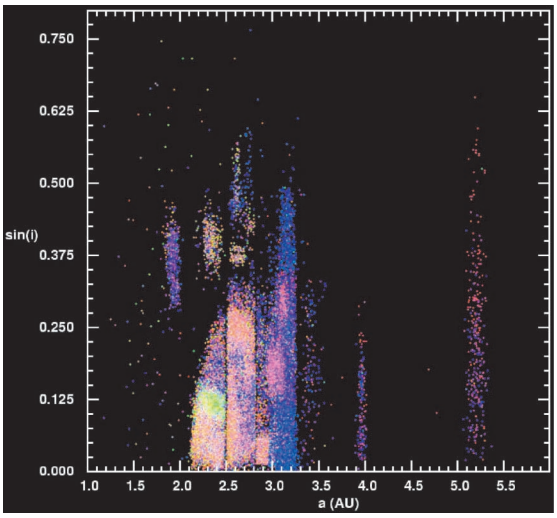

Figure 1. The dots show the osculating orbital inclination versus semimajor axis distribution of 43 424 unique moving objects detected by the SDSS, and matched to objects with known orbital parameters listed in Bowell's ASTORB file (these data are publicly available in the third release of the SDSS Moving Object Catalogue. The dots are colour-coded according to their colours measured by SDSS (see I02a for details, including analogous figures constructed with proper orbital elements). Note that most main-belt asteroid families have distinctive colours. Jovian Trojans asteroids are found at $a \sim 5.2$ au, and display a correlation between the colour and orbital inclination (objects with high inclination tend to be redder, see Section 4).

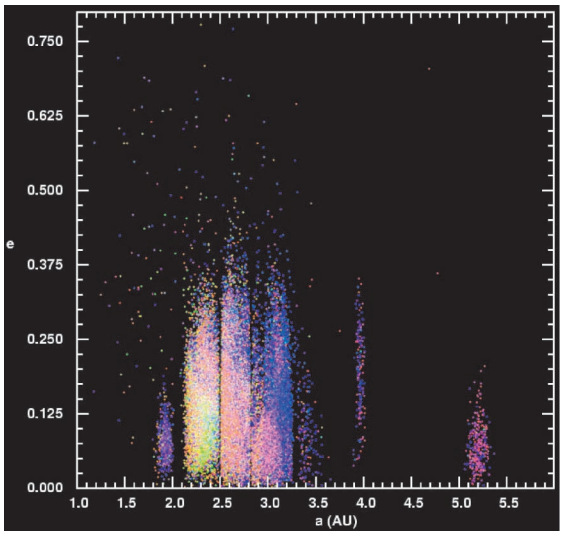

Figure 2. Analogous to Fig. 1, except that here the orbital eccentricity versus semimajor axis distribution is shown. Note that there is no discernible correlation between the colour and eccentricity for Jovian Trojan asteroids.

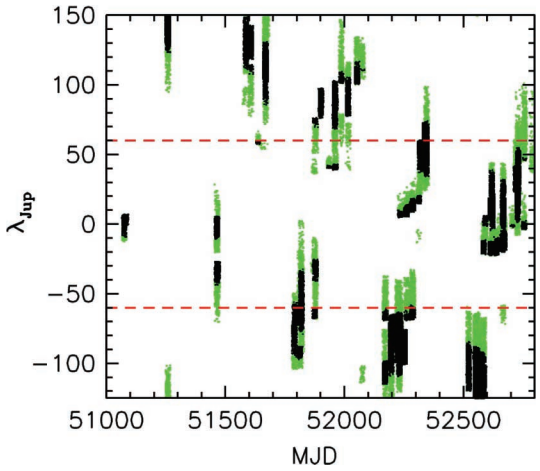

Figure 3. The distribution of the longitude of ∼440 000 9 × 13 arcmin^2 large SDSS observing fields in a coordinate system centre on Jupiter and aligned with its orbit, as a function of observing epoch (green symbols). Fields obtained within 25° from the opposition are marked by black symbols. The two dashed lines mark the relative longitudes of the L4 ($\lambda_{Jup} = 60°$, leading swarm) and L5 ($\lambda_{Jup} = -60°$, trailing swarm) Lagrangian points. Both swarms are well sampled in the third release of SDSS Moving Object Catalogue.

by Jedicke et al. (2004) and further discussed by Nesvorny et al. (2005). Multiple SDSS observations of objects with known orbital parameters can be accurately linked, and thus SDSS MOC also contains rich information about asteroid colour variability, discussed in detail by Szabó et al. (2004).

The value of SDSS data becomes particularly evident when exploring the correlation between colours and orbital parameters for main-belt asteroids. Fig. 1 uses a technique developed by I02a to visualize this correlation. A striking feature of this figure is the colour homogeneity and distinctiveness displayed by asteroid families. This strong colour segregation provides firm support for the reality of asteroid dynamical families. Jovian Trojans asteroids are found at $a \sim 5.2$ au, and display a correlation between the colour and orbital inclination (objects with high inclination tend to be redder). On the other hand, the colour and orbital eccentricity (see Fig. 2) do not appear correlated.

The distribution of the positions of SDSS observing fields in a coordinate system centred on Jupiter and aligned with its orbit is shown in Fig. 3. As evident, both L4 and L5 regions are well covered with the available SDSS data. There are 313 unique known objects (from ASTORB file) in SDSS MOC whose orbital parameters are consistent with Jovian Trojan asteroids (here defined as objects with semimajor axis in the range 5.0–5.4 au). Since SDSS imaging depth is about 2 mag deeper than the completeness limit of ASTORB file used to identify KTs, there are many more Trojan asteroids in SDSS MOC whose orbits are presently unconstrained. Nevertheless, they can be identified using a kinematic method described in the following Section.

3 SELECTION OF TROJAN ASTEROIDS FROM SDSS MOVING OBJECT CATALOGUE

The angular velocity of moving objects measured by SDSS can be used as a proxy for their distance determination and classification (see fig. 14 and appendix A in I01). For example, Jovian Trojan asteroids are typically slower than main-belt asteroids because their distances from Earth are larger (the observed angular velocity is dominated by the Earth's reflex motion). However, in addition to angular velocity, the selection algorithm must also include the longitudinal angle from the opposition, ϕ, because for large values of $|\phi|$ the main-belt asteroids can have angular velocity as small as Jovian Trojans. This behaviour is illustrated in Fig. 4.

We optimize criteria for selecting candidate Jovian Trojans with the aid of 482 observations of 313 Trojans from SDSS MOC that have known orbits extracted from ASTORB file (there are 43 424 unique objects with known orbits in the third release of SDSS MOC). These 482 observations are identified in orbital space using

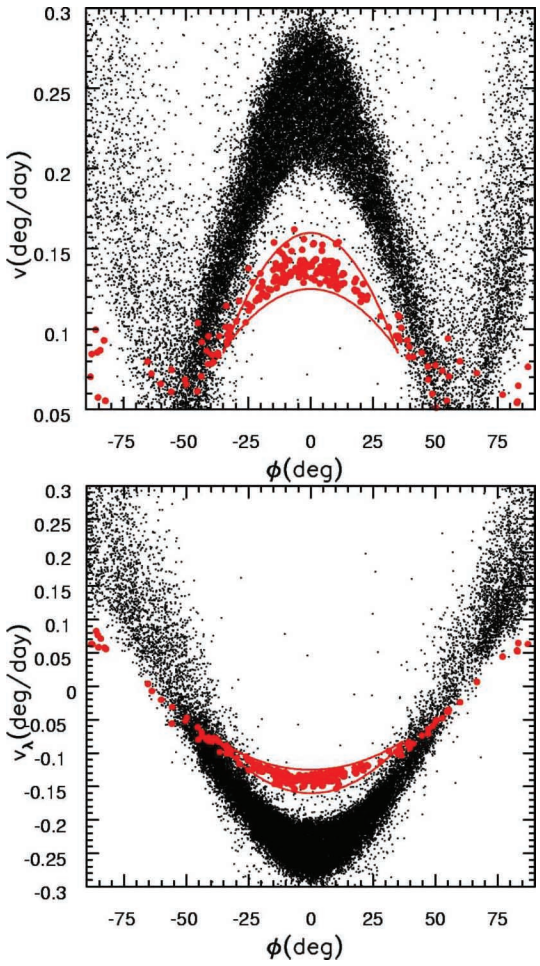

Figure 4. The basis for the kinematic selection of CT asteroids from SDSS Moving Object Catalogue. The small dots in the top panel show the magnitude of the measured angular velocity as a function of the longitudinal angle from the opposition for ∼43 000 unique objects with known orbits listed in the catalogue. The large dots show known Jovian Trojan asteroids. The lines show adopted selection criteria for CTs (see text). The bottom panel is an analogous plot and shows the measured longitudinal component of the angular velocity (in ecliptic coordinate system) as a function of angle from the opposition. The CTs are selected in the three-dimensional v–v_λ–ϕ space.

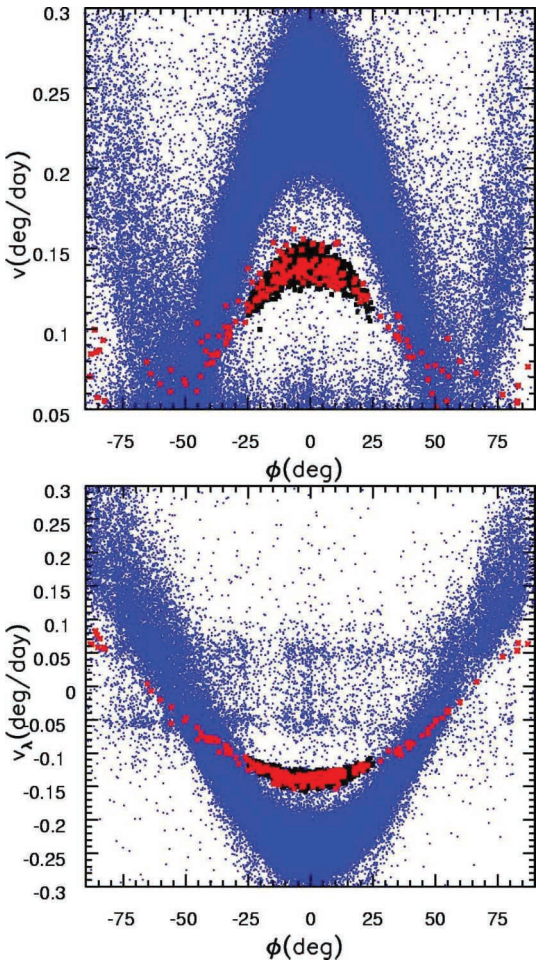

Figure 5. Analogous to Fig. 4, except that all ∼204 000 objects from SDSS Moving Object Catalogue are shown (blue dots). The CTs are shown by black symbols, and the KTs are overplotted as red symbols.

constraints $5.0 < a < 5.4$ au and $e < 0.2$, and hereafter referred to as the KTs. Of those, the majority (263) belong to the leading swarm.

We compare the angular velocity and ϕ distributions of these objects to those for the whole sample in Fig. 4. We find that the following selection criteria result in a good compromise between the selection completeness and contamination:

$$0.112 - \left(\frac{\phi}{180}\right)^2 < v < 0.155 - \left(\frac{\phi}{128}\right)^2, \quad (1)$$

$$-0.160 + \left(\frac{\phi}{134}\right)^2 < v_\lambda < -0.125 + \left(\frac{\phi}{180}\right)^2, \quad (2)$$

for observations with $-25 < \phi < 25$. That is, only observations obtained relatively close to the opposition can be used to select a sample with a low contamination rate by main-belt asteroids. The adopted velocity limits are in good agreement with those proposed by JTL.

When applied to all objects from SDSS MOC, this selection results in a sample of 1187 candidate Trojans (CTs), including 272 observations of known objects (see Fig. 5). Of the latter, eight objects have semimajor axis too small to be a Trojan asteroid, which implies a contamination rate of 3 per cent. SDSS MOC contains 297 observations of KTs obtained with $|\phi| < 25$, which implies that the kinematic selection method is 89 per cent complete. The 264 detections of KTs in the kinematically selected sample correspond to 191 unique objects. Therefore, 1187 detections in the candidate sample correspond to about 858 unique objects.

The contamination rate could be higher than 3 per cent because objects with known orbits tend to be brighter and thus have smaller measurement uncertainties for angular velocities than objects from the full candidate sample (for a detailed study of these errors and their correlation with other observables see I01). For this reason, we perform the following robustness test.

The above selection procedure does not include $\lambda_{\rm Jup}$, the longitudinal angle between an object and Jupiter. If the selection is robust, the $\lambda_{\rm Jup}$ distributions for the known and CTs should be similar. As discernible from Fig. 6, this is indeed the case and demonstrates that the contamination rate by non-Trojan asteroids in the candidate sample must be small. A similar conclusion is reached when comparing colour distributions (see below). We refer to this sample hereafter as the CTs.

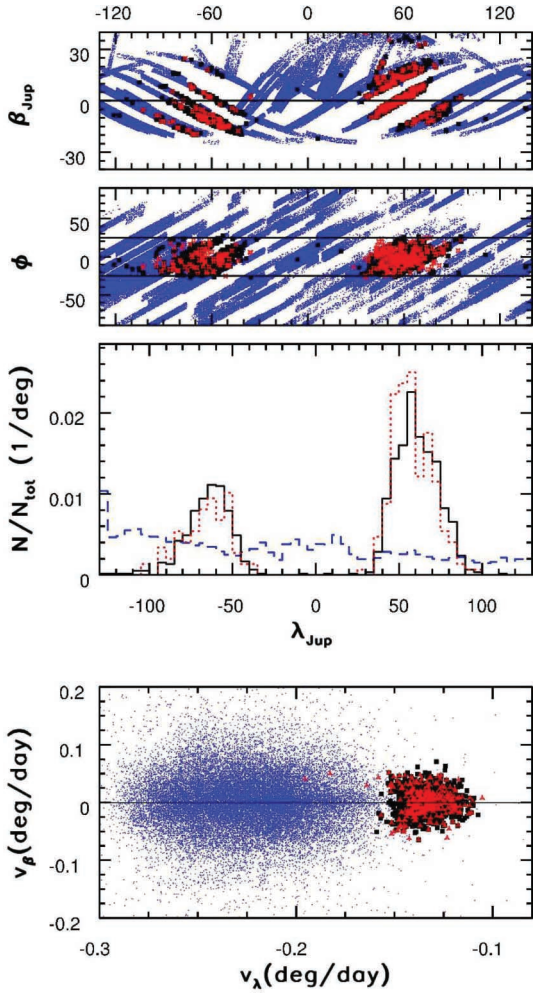

Figure 6. A test of the selection robustness. The top two panels show all the objects from SDSS MOC (small blue dots), the KTs (red dots) and the CTs (black squares), as observed on the sky, in Jupiter's coordinate system and in ϕ versus λ_{Jup} diagram. Although λ_{Jup} was not used in selection, the known and CTs have similar λ_{Jup} distributions (the third panel from top, dotted and solid histograms, respectively), and different than for the whole sample, dominated by main-belt asteroids (dashed line). Note that these λ_{Jup} distributions are not corrected for the selection biases due to inhomogeneous coverage of λ_{Jup}–β_{Jup} plane (which are presumably similar for both known and candidate objects), and thus are not representative of the true distribution. The bottom panel compares the angular velocity distributions of Trojans and main-belt asteroids.

4 ANALYSIS OF THE PROPERTIES OF TROJAN ASTEROIDS

Using the sample of CT asteroids selected as described above, here we analyse their distribution in the three-dimensional size–colour–inclination space, both for the full sample and separately for each swarm. The large size of the selected candidate sample allows accurate measurements of this distribution, and represents an especially significant improvement over the previous work when studying colour distribution. The two largest homogeneous studies of spectral properties of Jovian Trojans are by Jewitt & Luu (1990) and B04. Jewitt & Luu (1990) obtained spectra of 32 Trojans and found that they are remarkably similar to cometary spectra. Bendjoya et al. (2004) obtained spectroscopic observations for 34 objects and, together with older observations, produced a sample of 73 objects. Therefore, accurate colour information for over a thousand objects discussed here represents a substantial improvement.

4.1 The numbers of asteroids in L4 ad L5 swarms

It is usually assumed that the leading (L4) and trailing (L5) swarms contain similar number of asteroids down to the same size limit (e.g. JTL). Although the number of *known* objects in L4 and L5 differ (e.g. as listed in Bowell's ASTORB file), this asymmetry is usually dismissed as due to complex selection biases in the sample of Trojans with known orbits (e.g. Marzari et al. 2001). On the other hand, Pál & Süli (private communication) find using numerical simulations that the perturbations by Saturn produce different stability regions for L4 and L5. This effect is suspected to cause about a factor of 2 population size difference between the leading and trailing swarms. Therefore, it seems worthwhile to examine the number ratio for the two swarms implied by the SDSS data.

The top panel in Fig. 7 shows the observed surface density map of CT asteroids in Jupiter's coordinate system. There are 1.9 times more objects with $\lambda_{Jup} > 0$ than with $\lambda_{Jup} < 0$ (this asymmetry is already easily discernible in histograms shown in Fig. 6). However, this map does not reveal true density distribution because selection biases are strong even when using a homogeneous survey such as SDSS. The most important selection effect is the varying number of SDSS observations as a function of position relative to Jupiter, as shown in the middle panel.[3] It is the ratio of these two maps that is the best estimate of the underlying distribution of Trojan asteroids. This map is shown in the bottom panel in Fig. 7.

It is still not straightforward to use the counts from this corrected map to assess the number–count ratio for the two swarms. The reason is that the SDSS coverage of the λ_{Jup}–β_{Jup} plane is not symmetric with respect to $\lambda_{Jup} = 0$, and thus the counts cannot be simply summed up and compared. At the same time, the shape of the underlying distribution in the λ_{Jup}–β_{Jup} plane is not known.

We use two different methods to solve this problem. The first one assumes that the *shape* of the true distribution of Trojan asteroids in the λ_{Jup}–β_{Jup} plane is symmetric with respect to $\lambda_{Jup} = 0$ and $\beta_{Jup} = 0$, and the second one estimates this shape using a sample of KTs and normalizes it using the CT sample.

Although the coverage of the λ_{Jup}–β_{Jup} plane by the available observations is fairly sparse, there is sufficient overlap of regions with the same $|\beta_{Jup}|$ and $|\lambda_{Jup}|$ to compute the number ratio for the two swarms. With the assumption of symmetry with respect to $\lambda_{Jup} = 0$ and $\beta_{Jup} = 0$, we determine that the leading-to-trailing number ratio is 1.8 ± 0.2 (weighted average of all pixels). *It appears that the leading swarm has almost twice as many objects as the trailing swarm.*

The accuracy of the number–count ratio estimate can be increased when the shape of the λ_{Jup}–β_{Jup} distribution is assumed to be known (because all the data are used). We determined this shape using a sample of 1178 KT asteroids from ASTORB file. Their distribution in the λ_{Jup}–β_{Jup} plane is shown in the top panel in Fig. 8. We find that the shape of this distribution is well described by two two-dimensional Gaussians centred on $\beta_{Jup} = 0^\circ$ and $\lambda_{Jup} = \pm 60^\circ$, with the widths ($\sigma$) of 9° and 14°, for β and λ, respectively.[4] Using this

[3] Here we assume that the depth of SDSS imaging is constant, which is true to within several tenths of a magnitude.

[4] The errors for these estimates are not larger than ∼0.5 and indicate that the distribution of Trojans on the sky is not circularly symmetric around L4 and L5 points, as assumed by JTL.

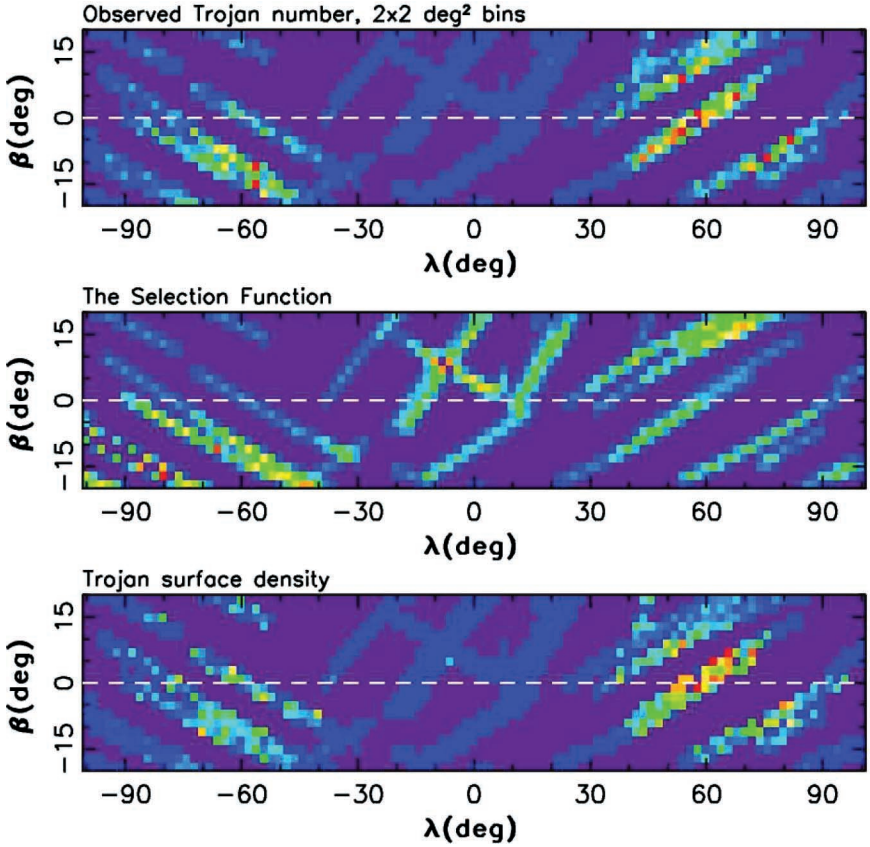

Figure 7. The top panel shows the observed surface density map (number of detected objects per 4 deg^2 large bin) of CT asteroids in Jupiter's coordinate system. The middle panel shows the number of SDSS fields observed in each bin (i.e. the selection function), and the bottom panel shows the corrected surface density of Trojans (the ratio of the maps in the top and middle panels). The values are shown on a linear scale, increasing from blue to red (i.e. no objects are found in blue strips). The maximum value (coded red) in the top panel is 20 (Trojans per 4 deg^2 large bin), 3.7 in the middle panel (SDSS observations per position, averaged over bin) and 5 (Trojans per deg^2, averaged over 4 deg^2 large bin). The purple (dark) regions contain no data.

shape, we fit the overall normalization for each swarm separately (i.e. two free parameters) and obtain the leading-to-trailing number ratio of 1.6 ± 0.1. The best-fitting model is shown in Fig. 8, as well as the residual map. With the assumption that the $\lambda_{\rm Jup}$–$\beta_{\rm Jup}$ distribution does not depend on size, this is our best estimate for the relative number count normalization for the two swarms. It is reassuring that we obtained a statistically consistent result using the first method. We emphasize that there is no discernible difference in the shape of the spatial distribution of objects from the two swarms.

Interestingly, this number ratio is about the same as the leading-to-trailing ratio of Trojans with known orbits in Bowell's ASTORB file. Although the selection effects are typically invoked to explain this asymmetry, it instead appears to be a real effect (we show below that the sample of KTs is indeed fairly complete to $r \sim 19.5$). On the other hand, the number ratio of asteroids in the two swarms could be dependent on object's size, and the SDSS sample extends to smaller sizes than ASTORB file. We address this possibility in the next section.

4.2 Apparent and absolute magnitude distributions

The differential apparent r-band magnitude distributions (for Trojans, Johnson's $V \sim r + 0.25$) for KTs and CTs are shown in the top panel in Fig. 9. The KT sample is complete to $r \sim 19.5$, and the CT sample is complete to $r \sim 21$. The formal cut-off for inclusion of moving objects in the SDSS MOC is $r < 21.5$. A slightly brighter completeness limit for Trojans can be understood as the removal of objects from a fairly narrow velocity space due to velocity errors (see fig. 6 from I01). Because the CT sample is complete to a ∼1.5 mag deeper limit, it contains ∼4 times more objects. It is noteworthy that the high completeness of KT sample indicated by the SDSS data (i.e. the counts are practically identical for $r < 19.5$) argues that selection effects *cannot* be invoked to explain the L4–L5 asymmetry in the number counts of Trojans with known orbits listed in Bowell's ASTORB file.

In order to investigate the dependence of various quantities (such as counts and colours) on object size, we transform apparent magnitudes to absolute magnitudes as follows. The dependence of apparent magnitude in the Johnson V band on absolute magnitude, H, distance from Sun, R, distance from Earth, Δ, and viewing (phase) angle, α, can be expressed as

$$V(R, \Delta, \alpha) = H + 5\log(R\Delta) + F(\alpha). \quad (3)$$

Here $V(R, \Delta, \alpha) = r + 0.44(g - r)$ is synthesized from SDSS measurements, $F(\alpha)$ is the phase function, and H includes the dependence on diameter D (in km) and the V-band albedo, p_V,

$$H = 19.14 - 2.5\log\left(\frac{p_V}{0.04}\right) - 5\log(D). \quad (4)$$

Note that formally $V(1, 1, 0) = H$. Given R and ϕ, Δ and α can be found from

$$\Delta^2 + 2\Delta\cos(\phi) + 1 = R^2 \quad (5)$$

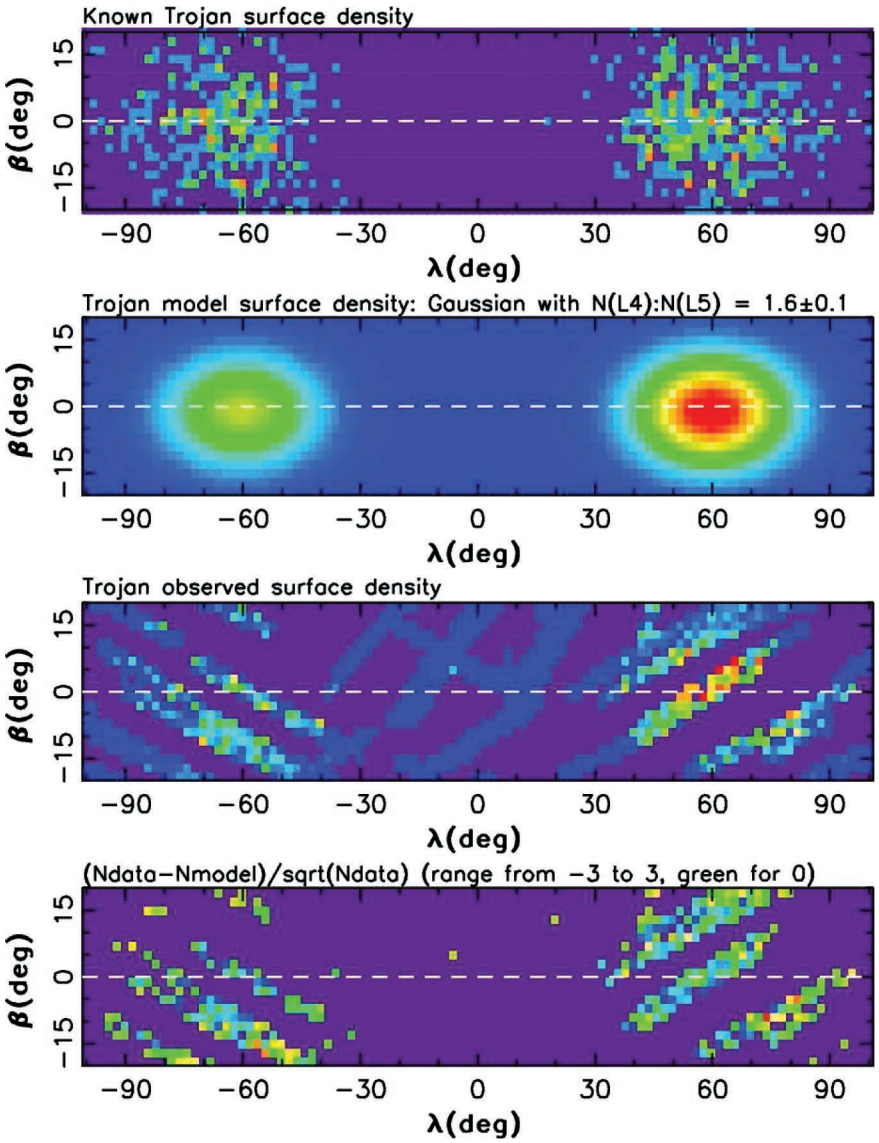

Figure 8. The top panel shows the observed surface density of KT asteroids from Bowell's ASTORB file, analogously to Fig. 7. The distribution for each swarm is well described by a two-dimensional Gaussian. The second panel shows a model distribution that has the same *shape* as the Gaussian distribution implied by the top panel, but normalized to the observed counts of SDSS CT (for each swarm separately), shown in the third panel with the same colour scheme (red corresponds to 5 objects per deg^2). The best-fitting L4:L5 number ratio is 1.6 ± 0.1. The difference between the observed counts and this model distribution, normalized by the Poisson error bars, is shown in the bottom panel (the purple regions contain no data). The value of χ^2 per degree of freedom is 1.15.

and

$$\alpha = \phi - \arccos\left(\frac{1 + \Delta\cos(\phi)}{R}\right). \quad (6)$$

When applying this procedure to observations discussed here, R and $F(\alpha)$ are not known. We adopt[5] $R = 5.2$ au and model the phase function as $F(\alpha) = k\,|\alpha|$. Therefore,

$$H \sim V(1, 1, 0) = V(1, 1, \alpha) - k|\alpha|. \quad (7)$$

In order to determine coefficient k, we used KT asteroids observed at low latitudes ($|\beta| < 10$). A least-squares best fit to the observed dependence of $V(1, 1, \alpha) - H$ on $|\alpha|$ gives $k = 0.066 \pm 0.018$. To the zeroth order, the transformation from apparent to absolute magnitudes for Trojans observed close to the opposition amounts to a shift of about 7 mag. In order to distinguish absolute magnitude for objects with known orbits from the estimates evaluated here, we will refer to H and $V(1, 1, 0)$ for KT and CT samples, respectively.

It is noteworthy that the intercept of the best-fitting line discussed above (see Fig. 10) is consistent with 0. This shows that the V-band magnitudes synthesized from SDSS photometry and H magnitudes for Trojans listed in ASTORB file are expressed on the same photometric system. This appears not be the case for a significant fraction of main-belt asteroids whose magnitudes (that are simply adopted from a variety of asteroid surveys) can have systematic errors as large as 0.5 mag (for more details see J02). The rms width of the residuals distribution shown in the bottom panel in Fig. 10 is

[5] I01 developed a method for estimating heliocentric distance of asteroids from their angular velocity measured by SDSS that is accurate to about 10 per cent for main-belt asteroids. For Trojans, which have larger velocity errors, a smaller error is introduced by assuming a constant R.

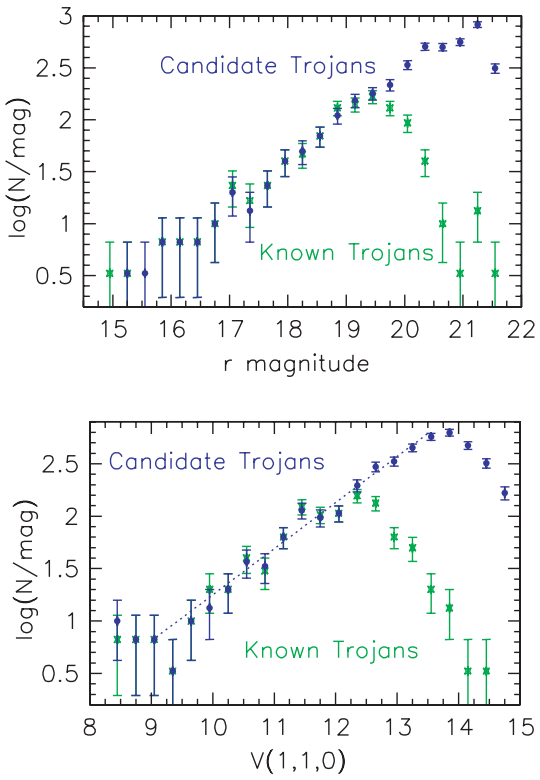

Figure 9. The top panel shows the differential SDSS *r*-band distributions for known (squares) and candidate Jovian Trojan asteroids (circles). The SDSS candidate sample is ∼1.5 mag deeper than the sample of known objects. The bottom panel compares the differential absolute magnitude distributions in the Johnson's *V* band. The dashed line is added to guide the eye and has the slope of 0.44. The SDSS data suggest that practically all Trojans brighter than $V(1, 1, 0) \sim 12.3$ ($r \sim 19.5$), or approximately larger than 20 km, are already discovered and listed in ASTORB file.

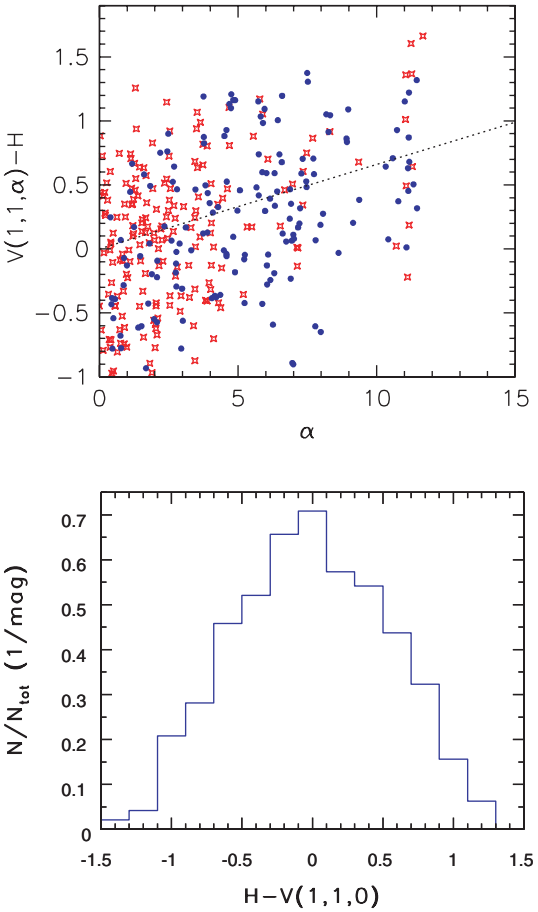

Figure 10. The calibration of phase effects on observed magnitudes. The top panel shows the distance-corrected magnitudes as a function of phase for KTs observed at small latitudes ($|\beta| < 10$). Two different symbols corresponds to objects from L4 (star) and L5 (dot) swarms. The dotted line shows a best linear fit discussed in the text. The bottom panel shows a histogram of the scatter around this best fit.

0.3 mag, and represents an upper limit for the errors of our method for estimating $V(1, 1, 0)$ (e.g. photometric and other errors for H listed in ASTORB file and intrinsic object variability probably also contribute).

The bottom panel in Fig. 9 compares the differential absolute magnitude distributions in the Johnson's V band for known and CTs. The SDSS data suggest that practically all Trojans brighter than $V(1, 1, 0) \sim 12.3$, or those with diameters approximately larger than 20 km, are already discovered.

We find that the differential absolute magnitude distribution is well described by

$$\log(N) = C + \alpha H \tag{8}$$

with $\alpha = 0.44 \pm 0.05$. This implies a differential size distribution index of $q = 5\alpha + 1 = 3.2 \pm 0.25$, valid for $9 < H < 13.5$. This value is in good agreement with JLT, who obtained $q = 3.0 \pm 0.3$ using about 10 times smaller sample, and with Yoshida & Nakamura (2005), who obtained $q = 2.9 \pm 0.1$ using a sample of 51 objects.

We use the counts of the presumably complete bright ($H < 12$, see Fig. 9) subsample of KTs from ASTORB file to normalize the *cumulative* counts

$$\log(N_{\rm cum}) = 2.9 + 0.44\,(H - 12). \tag{9}$$

Assuming $p_V = 0.04$ (Fernández et al. 2003), $D = 1$ km corresponds to $H = 19.14$. The above result implies that there are about 1 million Jovian Trojans larger than 1 km, to within a factor of 2 (uncertainty comes from the error in α and extrapolation over 5 mag; in addition, this normalization scales with the albedo approximately as $\propto 0.04/p_V$). This estimate could be up to a factor of 2 too high if Trojans size distribution becomes shallower for objects smaller than ∼5 km, as was found for main-belt asteroids (see I01), and is suggested for Jovian Trojans by Yoshida & Nakamura (2005). These results are in good agreement with the normalization obtained by JTL and imply that *there are about as many Jovians Trojans as there are main-belt asteroids down to the same size limit.*

In previous section, we demonstrated that L4 has a significantly larger number of objects than L5. To examine whether, in addition to this difference in overall normalization, the *slope* of the size (i.e. H) distribution is different for the two swarms, we separately analysed their counts. The slope of the size distributions for both the CTs (Fig. 11) and for KTs (Fig. 12) are the same within measurement uncertainties (with the slope error ∼0.05). Note that the L4-to-L5 count ratios shown in the bottom panel in Figs 11 and 12 are different from the value of 1.6 discussed in Section 4.1 because $\lambda - \beta$ selection effects (which are not a function of size) are not taken into account.

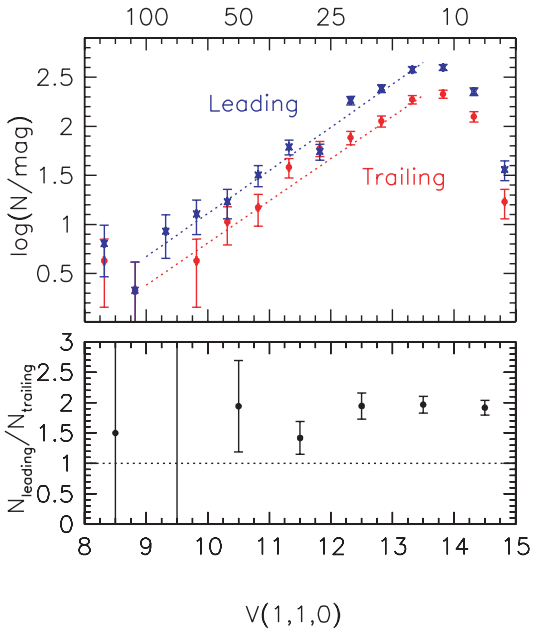

Figure 11. The top panel compares the *differential* distributions of estimated absolute magnitudes in the Johnson *V* band for CTs separated into leading and trailing swarms. The counts have indistinguishable slopes, but the overall normalization is different. The bottom panel illustrates this difference by showing the ratio of *cummulative* counts for the two swarms. Note that within errors this ratio does not depend on absolute magnitude, or equivalently size, as marked on top (diameter in km).

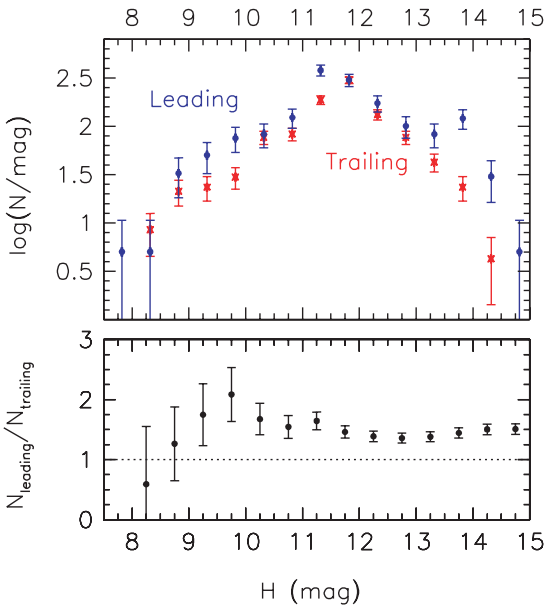

Figure 12. Analogous to Fig. 11, except that *all* KTs listed in Bowell's ASTORB file are included, and that absolute magnitude estimator $V(1, 1, 0)$ is replaced by the measured value H. Note that the leading swarm has ∼1.5 times more objects than the trailing swarm at the completeness limit ($H \sim 12$).

4.3 Colour distribution

One of the main advantages of the sample discussed here are accurate colour measurements for a sample about two orders of magnitude larger than available before. Together with robust knowledge about the colour distribution of main-belt asteroids in the SDSS photometric system (I01, I02a), we are in a position to compare the colours of the two populations with an unprecedented level of detail.

We first correct colour measurements for the phase effects using a linear colour versus phase angle approximation discussed in Section 4.2. We obtained the following best-fitting relations for the colours corrected to zero phase angle

$$(g-r)_c = (g-r) - 0.0051\,|\alpha|, \tag{10}$$

and

$$(r-i)_c = (r-i) - 0.0056\,|\alpha|, \tag{11}$$

with the coefficient errors of about 0.001 mag deg^{-1}. No significant correlation with the phase angle was detected for the $i-z$ colour, and too few objects have accurate $u-g$ colour measurement to attempt a robust fit. As the mean value of $|\alpha|$ is about 2°, these corrections are small compared to photometric accuracy.

The colour distribution of Trojan asteroids is compared to the colour distribution of main-belt asteroids in Fig. 13. The mean colours and their s.d. (not the error of the mean!) for CTs with colour errors less than 0.05 mag are $u-g = 1.45, 0.08, g-r = 0.55, 0.08, r-i = 0.22, 0.10$ and $i-z = 0.13, 0.11$ (for reference, these colours correspond to Johnson's $B-V = 0.73, V-R = 0.45$ and $R-I = 0.43$, using the photometric transformations from Ivezić et al. 2007; these values are in good agreement with previous work, e.g. Fornasier et al. 2004; Dotto et al. 2006). The two distributions are different, with the difference maximized in the $i-z$ versus $r-i$ diagram. Using solar colours from I01, we compute the relative albedo for Trojan asteroids and compare it to the three dominant main-belt colour types in Fig. 14. As expected from previous work, Trojan asteroids are redder than main-belt asteroids at wavelengths longer than the visual band.

In addition to maximizing colour differences between Trojan and main-belt asteroids, the $i-z$ versus $r-i$ diagram is interesting because the distribution of CTs suggests bimodality. To quantify this effect in the subsequent analysis, we define a colour index which is a linear combination of the $r-i$ and $i-z$ colours:

$$t^* = 0.93\,(r-i) + 0.34\,(i-z) - 0.25, \tag{12}$$

with the phase-angle correction

The distribution of this colour index for known and CTs is compared to that of the main-belt asteroids in Fig. 15. The fact that the distributions for known and CTs are indistinguishable, while clearly different from that of the main-belt asteroids, is another demonstration of the robustness of kinematic selection method.

The t^* distribution for Trojan asteroids is bimodal. At first it appears that this bimodality is related to L4 versus L5 separation, as illustrated in Fig. 15. However, objects from L4 and L5 have different *observed* orbital inclination distribution due to observational selection effects (see Section 4.3.1). Instead, the differences in the L4 and L5 colour distributions are due to a colour–inclination correlation, as detailed below.

4.3.1 *Correlation between colour and orbital inclination*

As was already discernible in Fig. 1, the colour and orbital inclination for Jovian Trojan asteroids are correlated. This correlation is presented in a more quantitative way in the top panel in Fig. 16 and in Table 1. As evident, objects with large orbital inclination tend to be redder. For example, the median t^* colour is −0.01 for objects with inclination less than 10°, while it is 0.04 for objects

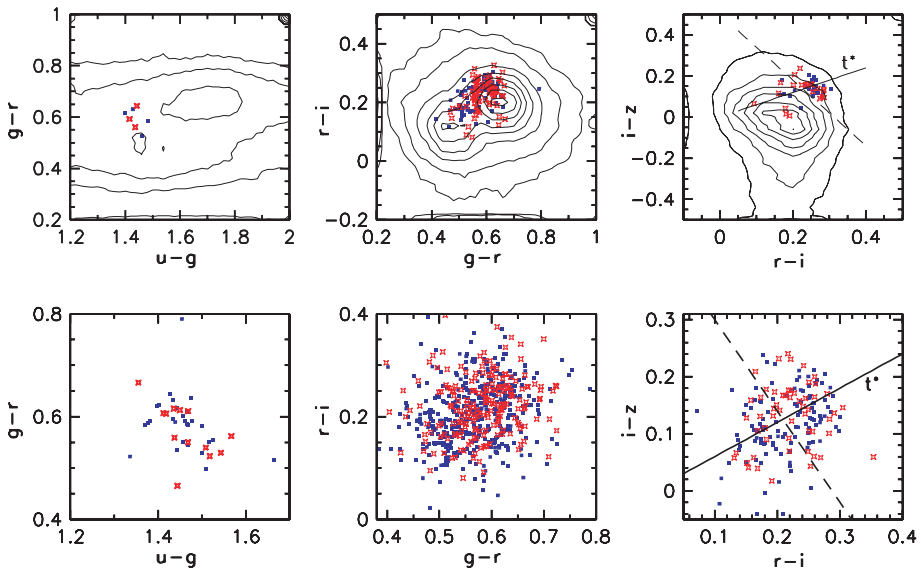

Figure 13. The top panels compare the colour distribution of the KT asteroids (symbols, blue for L4 and red for L5 swarm) to the colour distribution of main-belt asteroids (contours, linearly spaced). The bottom panels zoom in on the distribution of CTs, which is similar to that of the KTs. Measurement errors are typically less than 0.05 mag. The two lines in the *i*–*z* versus *r*–*i* diagrams shown on the right-hand panels define principal colours (see text).

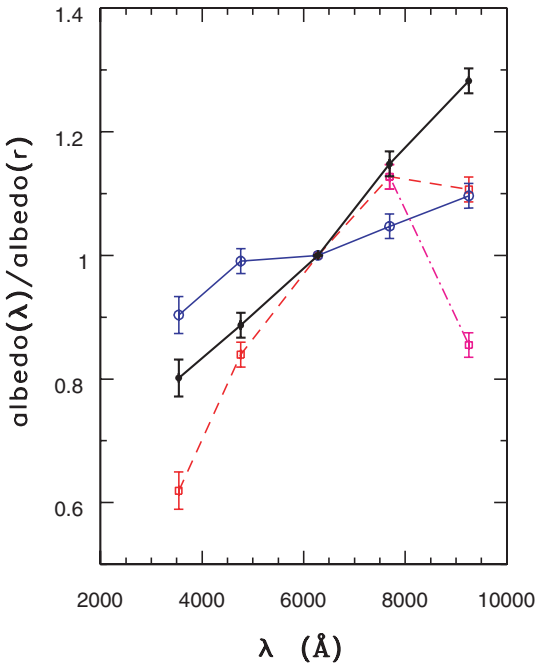

Figure 14. A comparison of the relative albedo for Trojan asteroids (black dots) and the relative albedo for the three dominant main-belt colour types (C type: blue circles, S type: red solid squares, V type: magenta open squares, for bands other than *z* same as S). Due to large sample sizes, errors reflect systematic uncertainties in SDSS photometric calibration.

with inclination greater than 10°, and 0.06 for those with inclination greater than 20°. While these differences are not large, they are detected at a statistically significant level (the formal uncertainties are smaller than 0.01 mag). Equivalently, the median inclination for objects with $t^* < 0$ is 8.9°, while it is 13.4 for the redder objects. The marginal colour distributions for subsamples selected by inclination are shown in the left-hand panel in Fig. 17.

The sample of CTs is much larger and fainter than the sample of KTs and can be used to test whether the colour–inclination correlation extends to smaller sizes. Since the orbital inclination is unknown for the majority of CTs,[6] we use as its proxy the latitude relative to Jupiter's orbit, β. When the sample of KTs is separated by $\beta = 6°$, 89 per cent of high-inclination and 66 per cent of low-inclination objects are correctly classified. As evident from the middle panel in Fig. 17, the differences in colour histograms for subsamples of KTs separated by β are still discernible, which justifies the use of β as a proxy for inclination. The colour histograms for CTs separated by β are shown in the right-hand panel in Fig. 17. As they look similar to the analogous histograms for KTs, we conclude that the colour–inclination correlation extends to smaller sizes.

Due to observational selection effects, the L5 subsample of KTs has a larger fraction of objects with large inclinations than the L4 subsample. This difference between L4 and L5, together with the colour–inclination correlation, results in differences between their t^* colour distributions discernible in Fig. 15. However, as shown in Fig. 18, once the objects are separated by inclination, or by β, this difference between L4 and L5 objects disappears. We conclude that there is no evidence for different colour–inclination correlations between the two swarms.

The similarity of the histograms shown in the middle and right-hand panels in Fig. 17 suggests that the colour–inclination correlation cannot be a strong function of object's size. Another 'slice' through the observed colour–inclination–size–swarm space is shown in Fig. 19. We find no strong correlation between the Trojan size and colour, except for a few large L4 objects with high inclination that have about ∼0.05 mag redder t^* colour. Indeed, these few

[6] I01 describe a method to estimate distance and inclination of moving objects from their observed apparent motions. While their method had satisfactory accuracy for studying main-belt asteroids, we found using a simple Monte Carlo simulation that it is not applicable here because the three times slower apparent motion of Trojans results in unacceptably large inclination errors.

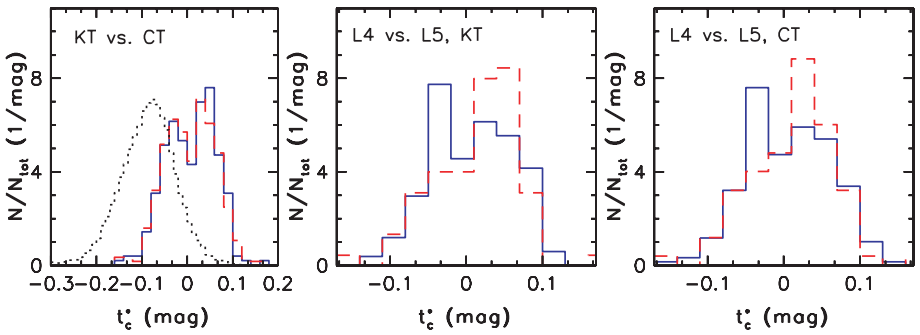

Figure 15. The left-hand panel compares the distribution of the synthetic colour index t^* for known (dashed line) and candidate (solid line) Trojan asteroids to that of the main-belt asteroids (dotted line). The middle and right-hand panels compares the t^* distribution separately for L4 (solid line) and L5 (dashed line) swarms. The differences between the two swarms are due to a colour–inclination correlation and different sampling of orbital inclinations due to observational selection effects (see Section 4.3.1).

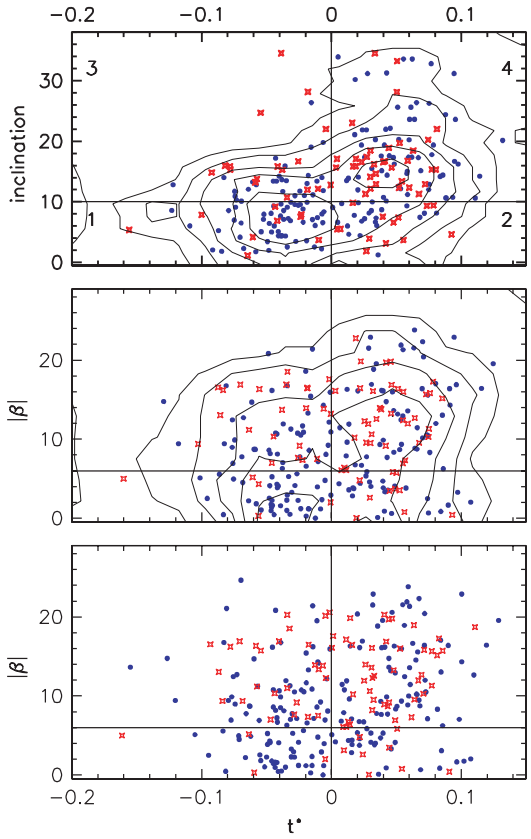

Figure 16. The top panel shows the distribution of KTs in the inclination versus colour diagram using linearly spaced contours. Individual objects are also shown and separated into L4 (blue dots) and L5 (red crosses) swarms. Note that L5 objects tend to have larger inclination due to observational selection effects. The middle panel is analogous, except that orbital inclination is replaced by its proxy β (latitude relative to Jupiter's orbit). The bottom panel is analogous to the middle panel, except that it shows CTs.

objects may be the reason for a claim by B04 that the spectral slope (i.e. colour) is correlated with size in the size range 70–160 km.

5 DISCUSSION AND CONCLUSIONS

The kinematically selected sample of candidate Jovian Trojan asteroids analysed here is complete at the faint end to $r = 21.2$ mag, approximately corresponding to 10 km diameter, with a contamination rate of only ∼3 per cent. Similarity of the longitude (relative to Jupiter) and colour distributions between known and CTs, and their difference from the distributions for main-belt asteroids which dominate the parent sample, strongly suggest that the kinematic selection is robust. The well-controlled selection effects, the sample size, depth and accurate five-band UV–IR photometry enabled several new findings and the placement of older results on a firmer statistical footing. The main results obtained here are as follows.

(i) The differential size distribution of Jovian Trojan asteroids follows a power law, $n(D) \propto D^{-q}$, with the power-law index of $q = 3.20 \pm 0.25$, in agreement with previous work (e.g. JTL). This value of q implies that the total mass is dominated by large objects. The overall normalization is tied to a complete sample of KTs and suggests that there are about as many Jovians Trojans as there are main-belt asteroids down to the same size limit, also in agreement with earlier estimates.

(ii) The same power-law size distribution provides a good description for both the leading (L4) and trailing (L5) swarm. Their spatial distribution on the sky can be described by two elliptical Gaussian distributions ($\sigma_\lambda = 14^\circ, \sigma_\beta = 9^\circ$) that have *different* normalization: *there are 1.6±0.1 more objects in the leading than in the trailing swarm.* The cumulative number of Jovian Trojan asteroids (per deg^2) as a function of absolute magnitude H and a position in Jupiter's coordinate system λ_J and β_J, in degree) can be estimated from

$$n(H, \lambda_J, \beta_J) = N_{\rm cum}(H) \frac{f(\lambda_J)}{2upi\sigma_\lambda\sigma_\beta} \, {\rm e}^{-\beta_J^2/2\sigma_\beta^2}, \qquad (13)$$

where $N_{\rm cum}(H)$ is given for $H < 13.5$ by equation (9), and

$$f(\lambda_J) = 0.62\,{\rm e}^{-(\lambda_J-60^\circ)^2/2\sigma_\lambda^2} + 0.38\,{\rm e}^{-(\lambda_J+60^\circ)^2/2\sigma_\lambda^2}. \qquad (14)$$

(iii) The two orders of magnitude increase in the number of objects with accurate colour measurements allowed us to demonstrate that Trojan asteroids have a remarkably narrow colour distribution (root mean scatter of only ∼0.05 mag) that is significantly different from the colour distribution of the main-belt asteroids.

(iv) We find that the colour of Trojan asteroids is correlated with their orbital inclination, in a similar way for both swarms, but appears uncorrelated with the object's size.

(v) We did not detect a size-inclination correlation.

These results have direct implications for the theories of Trojans origin. The detected difference in the normalization between leading and trailing swarms suggests that there was at least some

Table 1. The statistics of various colour indices show prominent inclination dependence. The subsets are selected by the inclination range, inc, N is the number of objects in each bin and Err is the s.e. of the mean.

inc	N	$\langle g-r\rangle$	Err	$\langle r-i\rangle$	Err	$\langle i-z\rangle$	Err	$\langle B-V\rangle$	Err	$\langle V-R\rangle$	Err	$\langle r-i\rangle$	Err	$\langle t\rangle$	Err
0–10	153	0.56	0.01	0.21	0.01	0.11	0.02	0.73	0.02	0.45	0.01	0.42	0.01	−0.02	0.01
10–20	227	0.58	0.01	0.24	0.01	0.13	0.01	0.75	0.01	0.47	0.01	0.47	0.01	0.01	0.01
20–30	71	0.60	0.02	0.26	0.01	0.16	0.01	0.77	0.02	0.48	0.01	0.48	0.01	0.04	0.01

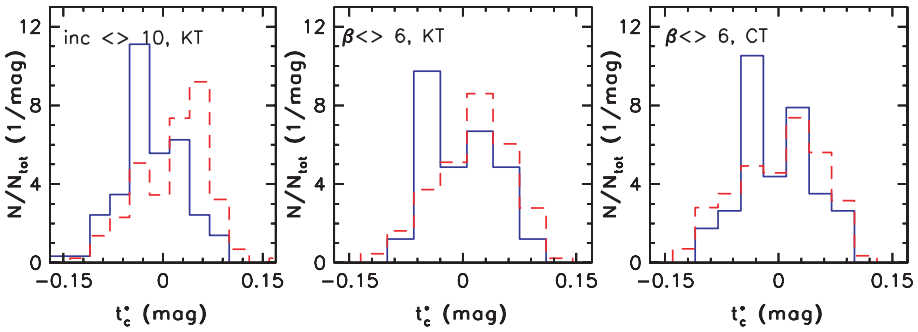

Figure 17. The left-hand panel compares the t^* colour distributions for subsamples of KTs separated by orbital inclination ($<10°$: solid line, $>10°$: dashed line. The middle panel is analogous, except that subsamples are separated by the observed latitude relative to Jupiter's orbit (β). The right-hand panel is analogous to the middle panel, except that it shows colour distributions for CTs. Note that objects with large inclinations and large β tend to have redder colours.

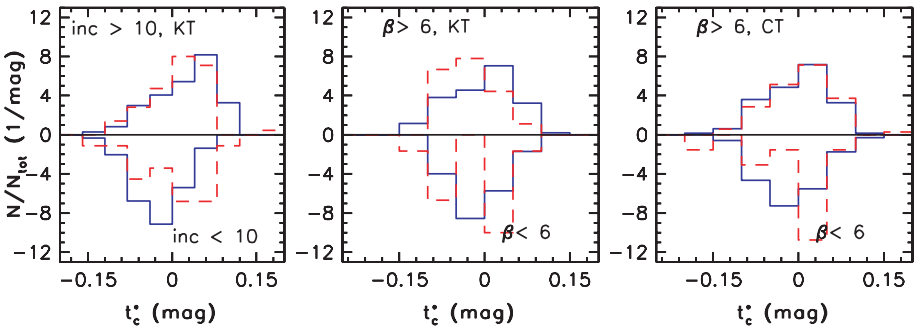

Figure 18. Analogous to Fig. 17, except that each histogram is separated into contributions from each swarm. The top histograms correspond to histograms shown by dashed lines in Fig. 17, and the bottom histograms to those shown by solid lines. Here solid line histograms correspond to L4 swarm and dashed line histograms to L5 swarm. As evident, once the objects are separated by inclination, or by β, the colour difference between L4 and L5 objects, visible in Fig. 15, disappears.

period during which their formation and/or evolution was different. Similarly, the colour–inclination correlation suggests that there must have been a process in the past which is responsible for the increased fraction of red objects at high orbital inclinations. Gas dynamics and planetary migration are good candidates for such a process, as recently discussed by Tsiganis et al. (2005). A possible explanation for this correlation is that when asteroids on the temporary eccentric orbits encounter the Sun, their minimal distance from the Sun is related to the inclination we observe today. In this picture the space weathering effects and volatization would vary with the inclination. A detailed analysis of these possibilities is beyond the scope of this paper and we leave it for future work.

While the increase in sample size enabled by SDSS is considerable, very soon new large-scale sky surveys, such as Pan-STARRS (Kaiser et al. 2002) and LSST (Tyson 2002), may obtain even more impressive samples, both in size, diversity of measurements and their accuracy. For example, LSST will scan the whole observable sky every three nights in two bands to a 5σ depth equivalent to $V = 25$ (about 2.5 mag deeper than SDSS). Using the size distribution determined here, we estimate that LSST, which may have its first light in 2014, will collect a sample of about 100 000 Jovian Trojan asteroids and provide *both* orbits, accurate colour measurements and light curves for the majority of them. A significant fraction (20–30 per cent) of this sample will be obtained by Pan-STARRS4, which is supposed to have its first light around 2009. These samples will undoubtedly reinvigorate both observational and theoretical studies of Jovian Trojan asteroids.

ACKNOWLEDGMENTS

We thank Elisabetta Dotto for a discussion that helped improve the presentation. This work has been supported by the Hungarian OTKA Grants T042509, the 'Magyary Zoltán' Higher Educational Public Foundation and the Szeged Observatory Foundation. We acknowledge generous support by Princeton University.

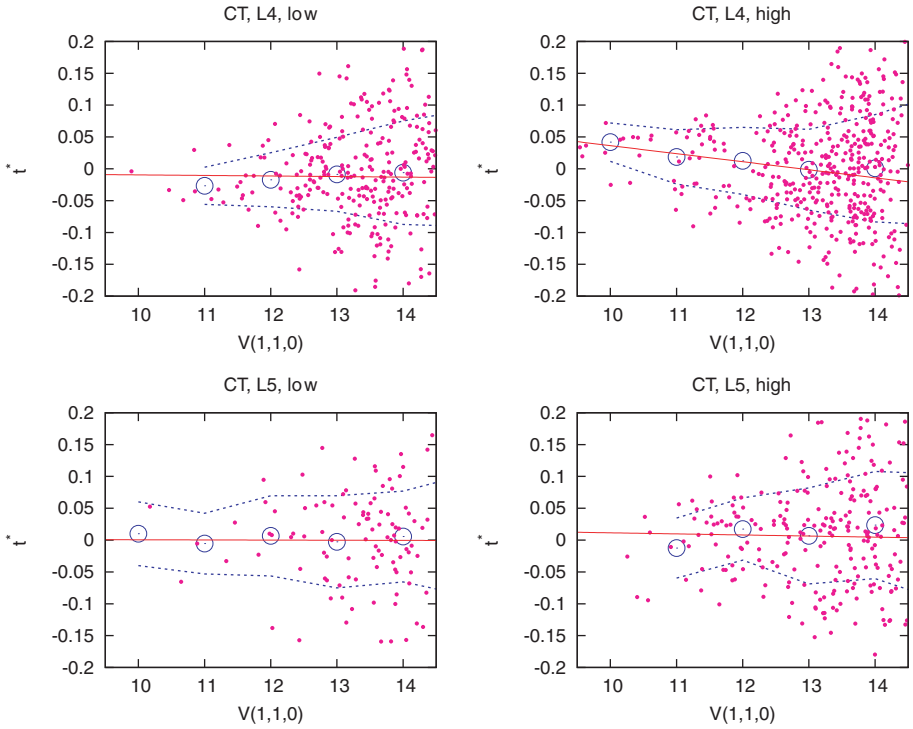

Figure 19. Colour–magnitude diagrams for subsamples of CTs separated into L4 (top) and L5 (bottom) objects, and further into low-inclination (left-hand panels) and high-inclination (right-hand panels) objects. Small dots represent individual objects and large circles are the median values of t^* colour in 1-mag wide bins of absolute magnitude. The 1σ envelope around the median values is computed from the interquartile range. Note the cluster of $V(1, 1, 0) < 11$ objects in top right-hand panel that have slightly redder objects than the rest of the sample.

Funding for the SDSS and SDSS-II has been provided by the Alfred P. Sloan Foundation, the Participating Institutions, the National Science Foundation, the US Department of Energy, the National Aeronautics and Space Administration, the Japanese Monbukagakusho, the Max Planck Society and the Higher Education Funding Council for England. The SDSS website is http://www.sdss.org/.

The SDSS is managed by the Astrophysical Research Consortium for the Participating Institutions. The Participating Institutions are the American Museum of Natural History, Astrophysical Institute Potsdam, University of Basel, University of Cambridge, Case Western Reserve University, University of Chicago, Drexel University, Fermilab, the Institute for Advanced Study, the Japan Participation Group, Johns Hopkins University, the Joint Institute for Nuclear Astrophysics, the Kavli Institute for Particle Astrophysics and Cosmology, the Korean Scientist Group, the Chinese Academy of Sciences (LAMOST), Los Alamos National Laboratory, the Max-Planck-Institute for Astronomy (MPIA), the Max-Planck-Institute for Astrophysics (MPA), New Mexico State University, Ohio State University, University of Pittsburgh, University of Portsmouth, Princeton University, the United States Naval Observatory and the University of Washington.

REFERENCES

Abazajian K. et al., 2003, AJ, 126, 2081
Bendjoya P., Cellino A., di Martino M., Saba L., 2004, Icarus, 168, 374 (B04)
Bowell E., 2001, Introduction to ASTORB, available from ftp://ftp.lowell.edu/pub/elgb/astorb.html
Dotto E. et al., 2006, Icarus, 183, 420
Fernández Y. R., Sheppard S. S., Jewitt D. C., 2003, AJ, 126, 1563
Fitzsimmons A., Dahlgren M., Lagerkvist C.-I., Magnusson P., Williams L. P., 1994, A&A, 282, 634
Fornasier S., Dotto E., Marzari F., Barucci M. A., Boehnhardt H., Hainaut O., de Bergh C., 2004, Icarus, 172, 221
Fukugita M., Ichikawa T., Gunn J. E., Doi M., Shimasaku K., Schneider D. P., 1996, AJ, 111, 1748
Gomes R. S., 1998, AJ, 116, 2590
Gunn J. E. et al., 1998, AJ, 116, 3040
Hogg D. W., Finkbeiner D. P., Schlegel D. J., Gunn J. E., 2002, AJ, 122, 2129
Ivezić Ž. et al., 2001, AJ, 122, 2749 (I01)
Ivezić Ž., Jurić M., Lupton R. H., Tabachnik S., Quinn T., 2002a, AJ, 124, 2943 (I02a)
Ivezić Ž., Jurić M., Lupton R. H., Tabachnik S., Quinn T., 2002b, Proc. SPIE, 4836, 98
Ivezić Ž. et al., 2004, Astron. Nachr. 325, 583
Ivezić Ž. et al., 2007, in Sterken C., ed., ASP Conf. Proc. Vol. 364, The Future of Photometric, Spectrophotometric and Polarimetric Standardization. Astron. Soc. Pac., San Francisco, p. 165
Jedicke R., Nesvorny D., Whiteley R., Ivezić Ž., Jurić M., 2004, Nat, 429, 275
Jewitt D. C., 1996, Earth, Moon & Planets, 72, 185
Jewitt D. C., Luu J. X., 1990, AJ, 100, 933
Jewitt D. C., Trujillo C. A., Luu J. X., 2000, AJ, 120, 1140 (JTL)
Jurić M. et al., 2002, AJ, 124, 1776 (J02)
Kaiser N. et al., 2002, Proc. SPIE, 4836, 154
Lupton R. H. et al., 2001, in Harnden F. R., Jr, Primini F. A., Payne H. E. M., eds, ASP Conf. Proc. Vol. 238, Astronomical Data Analysis Software and Systems X. Astron. Soc. Pac., San Francisco, p. 269
Lupton R. H., Ivezić Ž., Gunn J. E., Knapp G. R., Strauss M. A., Yasuda N., 2002, Proc. SPIE, 4836, p. 350
Marzari F., Scholl H., Murray C., Lagerkvist C., 2002, in Bottke W. F., Cellino A., Paolicchi P., Binzel R. P., eds, Asteroids III. Univ. Arizona Press, Tucson, p. 725

Milani A., 1999, Icarus, 137, 269
Morbidelli A., Levison H. F., Tsiganis K., Gomes R., 2005, Nat, 435, 462
Nesvorny D., Jedicke R., Whiteley R., Ivezić Ž., 2005, Icarus, 173, 132
Peale S. J., 1993, Icarus, 106, 308
Pier J. R., Munn J. A., Hindsley R. B., Hennesy G. S., Kent S. M., Lupton R. H., Ivezić Ž., 2003, AJ, 125, 1559
Shoemaker E. M., Shoemaker C. S., Wolfe R. F., 1989, in Binzel R. P., Gehrels T., Matthews M. S., eds, Asteroids II. Univ. Arizona Press, Tucson, p. 487
Smith J. A. et al., 2002, AJ, 123, 2121
Szabó Gy. M., Ivezić Ž., Jurić M., Lupton R., Kiss L. L., 2004, MNRAS, 348, 987
Tedesco E. F., 1989, in Binzel R. P., Gehrels T., Matthews M. S., eds, Asteroids II. Univ. Arizona Press, Tucson, p. 1090
Tedesco E. F., Cellino A., Zappalá V., 2005, AJ, 129, 2869
Tsiganis K., Gomes R., Morbidelli A., Levison H. F., 2005, Nat, 435, 462
Tyson J. A., 2002, Proc. SPIE, 4836, 10
York D. G. et al., 2000, AJ, 120, 1579
Yoshida F., Nakamura T., 2005, AJ, 130, 2900
Zellner B., Tholen D. J., Tedesco E. F., 1985, Icarus, 61, 355

This paper has been typeset from a TEX/LATEX file prepared by the author.